TB14

19th International Symposium of Ballistics, 7–11 May 2001, Interlaken, Switzerland

PENETRATION COMPARISON OF L/D=20 AND 30 MONO-BLOCK PENETRATORS WITH L/D=40 JACKETED PENETRATORS IN DIFFERENT TARGET MATERIALS

H.-J. Ernst[1], W. Lanz[2], T. Wolf[1]

[1] French-German Research Institute of Saint-Louis (ISL), P.O. Box 34, F-68301 SAINT-LOUIS CEDEX (France)
[2] Swiss Ordnance Enterprise Corp, Allmendstrasse 86, 3602 Thun, Switzerland

This presentation is to compare the flight behavior and the penetration performance of medium caliber L/D=40 jacketed penetrators in interesting ductile and brittle target materials to the ones of L/D=20 and L/D=30 mono-block rods at velocities of approximately 1550 m/s. The short mono-block projectile and the jacketed penetrator fly without recognizable bending vibrations. The jacketed penetrator yields a significantly higher penetration in RHA than the mono-block projectiles. Post mortem photographs and X-ray pictures of the crater forms in different brittle and ductile materials are presented. The jacketed penetrator yields in all brittle and ductile target materials under investigation the smallest space equivalence factors what means that it performs better than the mono-block projectiles.

INTRODUCTION

Projectiles of very high aspect ratios often show failure behavior because of structural integrity and stability problems during the acceleration and flight phases, such as flexure, buckling and/or bending vibrations which may also cause losses in terminal ballistic performance. One possibility to overcome these difficulties is the use of heavy metal penetrators reinforced by a steel sleeve, so-called jacketed penetrators [1]. Those penetrators have shown a good penetration performance especially in spaced armor in scaled experiments as well as in full scale tests. In spite of the high aspect ratio the heavy alloy core does not break, and the LOS-penetration is as high as in the reference RHA target [2].

The aim of this presentation is to demonstrate the penetration performance of medium caliber jacketed penetrators in interesting target materials and to compare it to the one of mono-block rods of different aspect ratios.

More information about results and comparisons of jacketed penetrators performances are found in [3, 4, 5, 6].

EXPERIMENTAL SET-UP

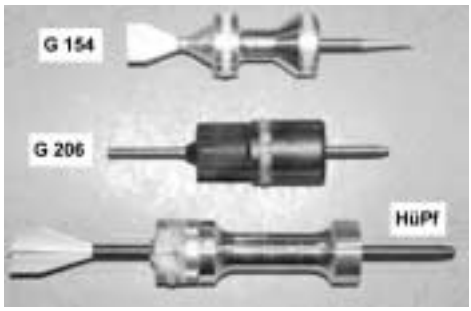

Figure 1: Photographs of the test projectiles.

Table 1: Dimensions and reference performance of the tested projectiles

projectile	L/D -1-	D mm	L mm	m_{pr}	v_z m/s	P_{ref} mm RHA	P_{ref}/L -1-
G 154	20	7.25	145	105	1550	126	0,87
G 206	30	6	180	90	1550	145	0,81
H Pf	40	6.5/8.3*	260	188	1550	184	0,71

* outer diameter of the reinforcing jacket made of maraging steel

Table 2: Penetrator materials

	tensile strength N/mm^2	density g/cm^3	Elongation %
ISL	1100	17.5	11
SWT	1700	17.5	>5

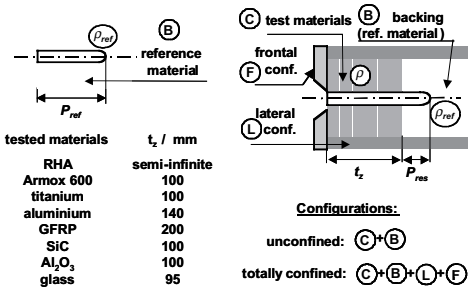

Figure 2: Target configurations and tested armor materials.

SW-Thun made jacketed penetrators with an aspect ratio of 40 have been tested at ISL in Saint-Louis (F) and at SW in Thun (CH) against materials such as RHA, titanium, aluminum, ceramics, glass, and high hardness steels. For comparison reasons these tests have been accompanied by additional experiments with ISL made mono-block tungsten heavy alloy rods with aspect ratios of 20 and 30. All projectiles have been accelerated at SWT in 38 mm or at ISL in 40 mm smooth barrel test guns up to velocities of approximately 1550 m/s.

In Fig. 1 photographic views of the three projectiles are given. Some important data are summarized in Tab. 1. Though the normalized penetration of the jacketed penetrators has the smallest value due to its higher L/D-ratio, its absolute penetration into RHA at 1550 m/s is significantly higher than the ones of the mono-block projectiles because of its higher length and energy.

All projectiles are made of tungsten heavy alloy. Some parameters of the penetrator materials used for the two mono-block and jacketed projectiles are seen in Tab. 2.

Fig. 2 shows a schematic drawing of the different target configurations for the DOP experiments as well as a list of the tested target materials and their thicknesses. The unconfined target consists of ductile material plates C being placed in front of the RHA backing B. The totally confined target is used for brittle materials only in order to simulate the self confinement of a material with infinite lateral dimensions. Therefore, lateral confinement plates L and a frontal confinement plate F have been added. The entrance hole ensures identical impact conditions for both configurations. The achieved penetration performances of the projectile in the tested target (t_z and P_{res}) are compared with the reference penetration in

RHA at the same velocity P_{ref}. These results are used to define a layer of the reference material of the thickness

$$t_{ref} = P_{ref} - P_{res} \tag{1}$$

which is equivalent (in terms of terminal ballistics) to the tested material of the thickness t_z. Now the space equivalence factor [6] can be defined as

$$F_s = \frac{t_{ref}}{t_z} \tag{2}$$

A comparison of different projectiles impacting a constant test target at approximately the same velocity can be done by using the space equivalence factor: the projectile which yields the lowest F_s-value has the highest penetration performance.

RESULTS

Reference Penetration

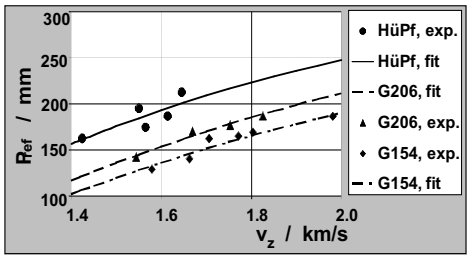

Figure 3: Reference penetrations in RHA.

In the first series of experiments, the three projectiles under investigation were tested in RHA in order to get the fit curves which were to be regarded as a reference for the further experiments with different inert armor materials. The diagram in Fig. 3 shows the experimental data as well as fit curves of the Lanz/Odermatt type [7] at impact velocities between 1400 m/s and 2000 m/s. The general fit equation is:

$$\frac{P_{ref}}{L} = a \cdot e^{-\left(\frac{b}{v_z}\right)^2} \tag{3}$$

Table 3: Lanz-Odermatt parameters

	G 154	G 206	Hüpf
a	2.379	2.076	1.478
b	1.554	1.509	1.328

In Tab. 3 the Lanz/Odermatt parameters of the three projectiles under investigation are summa-rized. It can be seen in Fig. 3 that the jacketed penetrator (HüPf) has a significantly higher penetration performance than the mono-block projectiles. As expected, the longer mono-block projectile

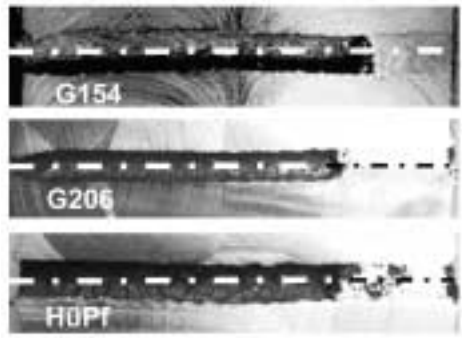

Figure 4: Craters in RHA (reference).

with the higher aspect ratio (G206, L/D=30) performs better than the shorter one (G154, L/D=20). In order to compensate for the experimental velocity scattering, the reference penetration is calculated with these fit curves for the measured impact velocity.

Only in RHA the craters are regular, straight and cylindrical. As will be shown later in more details, in aluminum and titanium the craters are less regular and varying in diameter and in direction.

Flight Behavior

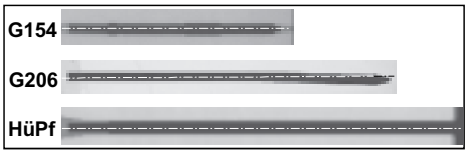

Figure 5: X-ray pictures of the flying projectiles.

Because of the well-known bending vibrations of high aspect-ratio projectiles there was a distinct interest to compare the flight behavior of the three projectiles under investigation. Fig. 5 shows exemplarily X-ray pictures of the three projectiles flying at a velocity of approximately 1550 m/s, taken 17 m in front of the barrel after the sabots had taken off. The short mono-block projectile and the jacketed one fly without any recognizable bending whereas the tip of the longer mono-block projectile is significantly bent downwards. Of course, this misalignment of the L/D=30 penetrator will have negative consequences for its penetration performance, as will be seen later-on.

Crater Forms

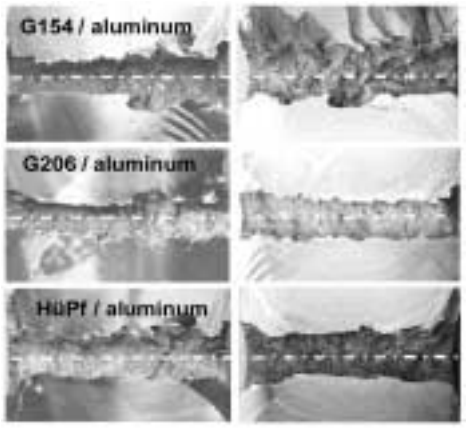

Figure 6: Aluminium craters.

In order to compare the penetration behavior, it has been tried to visualize the craters in the different target materials post mortem. As far as ductile materials were concerned, the target blocks have been cut in the vicinity of the crater axis. In Fig. 6 photographs of the aluminum craters are shown, the projectiles flying from the left to the right hand side. In the case of the G154, parts of the second plate broke off during the cutting , so the upper contour of the crater does not have the real crater shape. Nevertheless, it is seen that for all projectiles the crater has a smaller diameter in the entrance region. Later-on its cross section nearly remains constant. Plate interfaces as well as the end of the crater show additional material brake-outs caused by impedance variations. The diameters of the two mono-block projectiles are relatively similar in diameter, whereas the jacketed penetrator causes a crater with a significantly larger diameter.

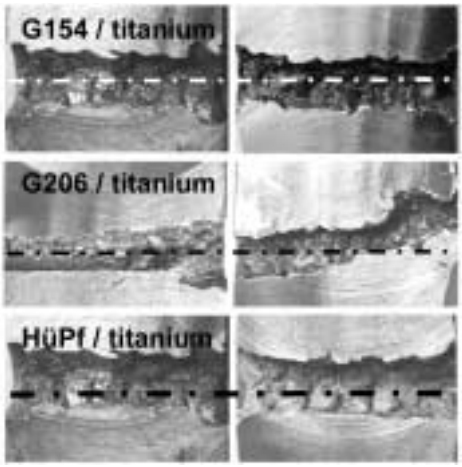

Figure 7: Titanium craters.

Table 4: Averaged crater diameters(mm).

	G 154	G 206	HüPf
aluminum	14.4	13.2	18.2
titanium	13.5	10.7	14.3
RHA	14.7	11.8	13.8

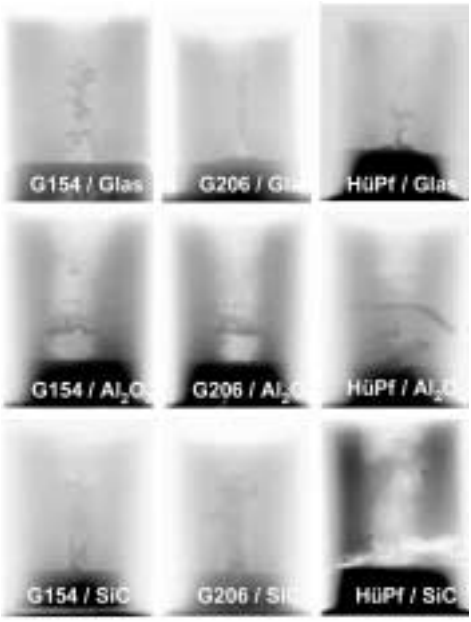

Figure 8: X-ray pictures of ceramic craters.

In Fig. 7 the craters in titanium are presented in the same way as before in aluminum. Here, the projectiles with the larger caliber cause the biggest crater diameters: G154 in the upper two and HüPf in the lower two pictures. The L/D=30 mono-block causes a crater which turns in the second plate to the upper side, what surely is a consequence of the bending vibrations mentioned before.

In Tab. 4 the averaged crater diameters in titanium and aluminum of all projectiles under investigation are compared to those in RHA. Two points may be pointed out: Firstly: Though there is a steel jacket of nearly 1 mm thickness which has only half of the density of tungsten, the jacketed penetrator yields in all of the tree materials the biggest averaged crater diameters. But if referred to the outer projectile diameter, it yields the smallest relative crater diameter. Secondly: Titanium and RHA have similar crater diameters what shows again the good protection performance of titanium [8].

The crater contours in totally confined brittle materials are more difficult to visualize. While opening the confinement boxes the shot ceramic blocks of glass, Al_2O_3 and SiC have been continuously stabilized by adding a liquid glue. There-after X-ray pictures have been taken which are summarized in Fig. 8. Though it is not possible to quantify the crater diameters, there are some interesting differences of the impact behavior between the three ceramics recognizable which seem to be common to the three projectiles under investigation.

In the case of glass the projectile material is concentrated to the crater axis. This special impact behavior has already been observed earlier and was explained by a crater implosion as a consequence of the phase transition occurring in this material after the impact [9]. In the Al_2O_3 craters the projectile material of all projectiles is mostly

found in the interstices between the tiles. Relatively big regions of lower density are visible with slightly different diameters, the smallest one corresponding to the G206. SiC shows a behavior in between the other two brittle materials: here the projectile material is also condensed near the crater axis showing a bigger diameter than in glass. The projectile remnants might form a sort of a hull which then should be similar to the crater contour during the impact.

Ballistic Equivalence Factors

As it was mentioned before, a comparison of different projectiles can be done by using the space ballistic equivalence factor (eq. 2): impacting the same target at the same velocity the projectile which yields the lowest F_S-value has the highest penetration performance.

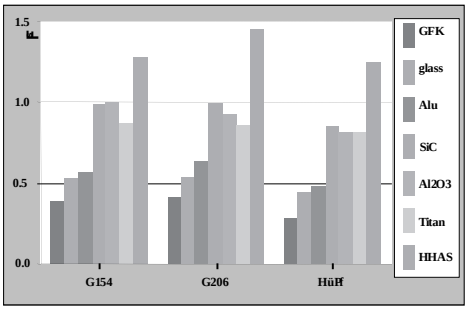

Figure 9: Material related space equivalence factors.

In Fig. 9 the experimentally achieved space factors are shown in form of a material related bar graph. The length of bars represents the size of the space equivalence factor for the different materials mentioned in Fig. 2. For each of the three projectiles under investiga-tion all materials are arranged from left to right according to their growing densities.

All projectiles show a more or less similar penetration behavior. It is obvious that the high hardness steel has the best protective power, the only target material which yields space gains of more than 1 for all projectiles. GFRP (GFK) has the smallest equivalence factors in the order of 0.4. Aluminum and glass reach F_S-factors around 0.5 having relatively small protective power differences. Another group of three materials, titanium, Al_2O_3 and SiC, shows a similar protective effect with equivalence factors higher than 0.8.

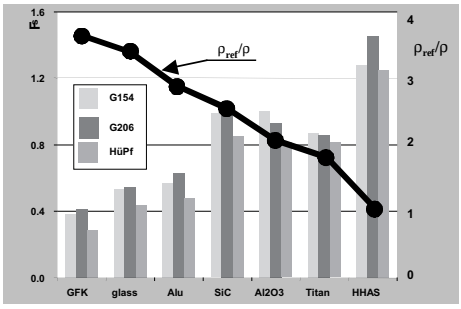

Figure 10: Projectile related space equivalence factors.

In the bar plot of Fig. 10 the bars denote the equivalence factors of the different projectiles arranged for the materials. The thick solid line with the dots for each material shows the density relation which is the quotient of reference material density divided by target material density. As the equivalence mass factor is equal to the product of space factor and density relation, it can indirectly be seen that low density materials such as GFRP (GFK) and glass get higher mass factors than high hardness steel or titanium.

At the first glance it is seen in Fig. 10 that the longer mono-block projectile has the highest F_S-factors with the exceptions of titanium and Al_2O_3. This means that the L/D=30 projectile mostly has the lowest penetration performances what surely will be a consequence of the above mentioned bending vibrations. The jacketed penetrator yields in all materials under investigation the smallest space equivalence factors what indicates that it performs better than the mono-block projectiles.

CONCLUSIONS

In opposite to the L/D=30 mono-block projectile the short mono-block projectile and the jacketed one fly without any recognizable bending vibrations.

In spite of the relatively small density steel jacket of nearly 1 mm thickness, the jacketed penetrator yields in the three ductile target materials the biggest averaged crater diameters.

The L/D=30 projectile mostly has the lowest penetration performances what surely will be a consequence of its bending vibrations. The jacketed penetrator yields in all materials under investigation the smallest space equivalence factors what means that it performs significantly better than the mono-block projectiles.

Summarizing, it is stated that jacketed penetrators are an enriching alternative in order to defeat brittle and ductile target materials for the use in light weight armor.

REFERENCES

1. Lanz W., Lehr H.F., “Craters Caused by Jacketed Heavy Metal Projectiles of Very High Aspect Ratios Impacting Steel Targets”, *Proceedings of the 16th Int. Symp. on Ballistics*, San Francisco, USA, 1996
2. Lanz W., Odermatt W., “Minimum Impact Energy für KE Penetrators in RHA Targets”, *Proceedings of the European Forum on Ballistics of Projectiles*, ISL, St.-Louis, France, 2000
3. Peskes G.J.J.M., “Evaluation of Jacketed Penetrators for Tank Ammunition”, *Proceedings of the 19th Int. Symp. on Ballistics*, Switzerland, 2001
4. Diederen A.M., Hoeneveld J.C., “Replica Scale Modeling of Long Rod Penetrators”, *Proceedings of the 19th Int. Symp. on Ballistics*, Switzerland, 2001
5. Fang H., Hölzle J., Knobel R., Lanz W., “Joining Jacket and Core in Jacketed Steel/Tungsten Penetrators”, *Proceedings of the 19th Int. Symp. on Ballistics*, Switzerland, 2001
6. Lanz W., Odermatt W., Dr. Weihrauch G., “Anti-Tank KE Projectiles: Development History, State of the Art, Trends”, *Proceedings of the 19th Int. Symp. on Ballistics*, Switzerland, 2001
7. Ernst H.-J., Merkel Th., “Zur Vereinheitlichung der Anwendung ballistischer Faktoren”, ISL RT 519/2000, 2000
8. Lanz W., Odermatt W., “Penetration Limits of Conventional Solid Propellant Guns, Kinetic Energy Projectiles”, *Proceedings of the 13th Int. Symp. on Ballistics*, Sweden, 1992
9. Gooch W.A., Burkins M.S., Ernst H.-J., Wolf T., “Ballistic Performance ot Titanium against Laboratory Penetrators with Aspect-Ratios of 10 or Greater”, *Proceedings of the 15th Int. Symp. on Ballistics*, Israel, 1995
10. Ernst H.-J., Hoog K., Wiesner V., “Ballistic Impact Behavior of Some Ceramics in Different Environments”, EURODYMAT 94 Conference, UK, 1994